Multivaluedness of the Luttinger-Ward functional in the fermionic and bosonic system with replicas

Aaram J. Kim [1,*] and Vincent Sacksteder, IV[2]

[1]*Department of Physics, King's College London, Strand, London WC2R 2LS, United Kingdom*

[2]*Department of Physics, Royal Holloway University of London, Egham, Surrey TW20 0EX, United Kingdom*

(Received 5 April 2019; revised manuscript received 4 February 2020; accepted 5 March 2020; published 31 March 2020)

We study the properties of the Luttinger-Ward functional (LWF) in a simplified Hubbard-type model without time or spatial dimensions, but with N identical replicas located on a single site. The simplicity of this $(0+0)d$ model permits an exact solution for all N and for both bosonic and fermionic statistics. We show that fermionic statistics are directly linked to the fact that multiple values of the noninteracting Green's function G_0 map to the same value of the interacting Green's function G; that is, the mapping $G_0 \mapsto G$ is noninjective. This implies that with fermionic statistics the $(0+0)d$ N-replica model has a multiply valued LWF. The number of LWF values in the fermionic model increases proportionally to the number of replicas N, while in the bosonic model the LWF has a single value regardless of N. We also discuss the formal connection between the N-replica model and the $(0+1)d$ Hubbard atom which was used in previous studies of LWF's multivaluedness.

DOI: 10.1103/PhysRevB.101.115146

I. INTRODUCTION

The Luttinger-Ward functional (LWF) [1,2] is the foundation of a variety of modern quantum many-body techniques. Dynamical mean-field theory (DMFT) [3] and its extensions [4–9] are derived from the LWF and have played an important role in studies of both idealized models and real materials [10,11]. Also based on the LWF are self-consistent diagrammatic methods such as the bold diagrammatic Monte Carlo method with different degrees of the dressing [12–15] and the self-consistent Hartree-Fock and GW methods [16].

Despite extensive usage of the LWF, rigorous tests of its formal validity have not been completed. The justification of the LWF is based on performing a Legendre transformation on the thermodynamic potential Ω with respect to the external single-particle source field [17–21]. Following Baym and Kadanoff, the transformed Ω becomes stationary as a functional of the interacting Green's function G [22,23]. The LWF is the universal part of the Baym-Kadanoff functional, which does not depend on the noninteracting part of systems. However, the Legendre transformation used to define the LWF depends sensitively on the mathematical properties of the thermodynamic potential Ω. If Ω is not both smooth and convex with respect to the external source field, then the Legendre transformation is not well defined, and the LWF's validity is thrown into doubt.

A recent study demonstrated the LWF's fragility, showing that the LWF of a simple model of a fermionic Hubbard atom with zero spatial dimensions plus the time dimension [i.e., $(0+1)$ dimensions], is a multivalued functional of G [24]. In other words, if G is held fixed, then two or more values of the LWF and of the self-energy Σ can be found which are consistent with the fixed value of G. Since the $(0+1)d$ Hubbard atom has a unique physical value of the self-energy Σ, the additional values produced by the LWF are unphysical. A multiply-valued LWF restricts the predictive power of formalisms since even a physical Green's function can lead to the unphysical self-energy.

The first report that the LWF is multivalued when applied to the $(0+1)d$ fermionic Hubbard atom used the bold diagrammatic Monte Carlo method and DMFT [24]. Following this watershed paper, several authors have performed detailed studies of the multivaluedness problem of the LWF. In order to obtain a qualitative understanding Ref. [25] introduced a simpler fermionic model where imaginary time is suppressed [a $(0+0)d$ model] and explained the qualitative behavior of the first unphysical branch. References [26,27] extensively investigated the functional space of the Green's function. Reference [28] found additional unphysical branches, implying that the LWF has an infinite number of values when applied to the $(0+1)d$ model and also found that one eigenvalue of the charge vertex diverges at the branching point of the LWF [28–31].

In spite of these extensive studies, the problem of the LWF's multivaluedness is still not thoroughly understood. It is not clear how general this problem is, or what the essential ingredients of the set of models for which the LWF produces multiple solutions are. Most importantly, the role of the fermionic statistics in the LWF has not been studied.

In the present paper we study the LWF's behavior of the $(0+0)d$ fermionic model which has been generalized to include N replicas on the single site. This N-replica generalization plays the role of connecting the $(0+0)d$ model [25] and the realistic $(0+1)d$ Hubbard atom, regarding the replica indices as the Matsubara frequencies. We discuss in detail the formal similarity between the N-replica model and the $(0+1)d$ Hubbard atom and to what extent the N-replica model can reproduce the multivaluedness properties observed in the Hubbard atom. We also study a model which is different in

*aaram.kim@kcl.ac.uk

only one respect: the N replicas obey bosonic statistics instead of fermionic statistics. We exactly solve both models, and we find a mathematical correspondence between the fermionic N-replica model and the bosonic N-replica model: the formula for the Green's function G of the bosonic N-replica model is exactly the same as that of the fermionic N-replica model with $-N$ substituted for N. This means that the bosonic results can be obtained from the fermionic results and vice versa by changing the sign of the replica count N. With these results in hand, we examine the number of possible values of the LWF as a function of N for strictly real G and also for complex G. In the fermionic model the number of values increases as a function of N with a staircase profile, while in contrast the bosonic model always has exactly one solution. In other words, in the N-replica model the multivaluedness of the LWF is caused specifically by fermionic statistics and is cured by using bosonic statistics. Examining the mathematical structure of the model, we find that the sign of the fermionic partition function $\mathcal{Z}$ changes as the single-particle potential is varied and that at each sign change the thermodynamic potential $\Omega = -\ln \mathcal{Z}$ is not smooth. In addition, Ω is, in general, not convex. These two properties result in the multiple values of the LWF. In contrast, in the bosonic case $\mathcal{Z}$ has a single sign, and Ω is both smooth and convex, resulting in a single-valued LWF.

II. MODEL AND METHOD

We introduce the $(0+0)d$ Hubbard model with N replicas, a single-particle potential μ, and a quartic interaction with strength U. The actions $\mathcal{S}_F$ and $\mathcal{S}_B$ of the fermionic and bosonic variants are

$$\mathcal{S}_F = \frac{U}{2}\left(\sum_{\alpha=1}^{N}\sum_{\sigma}\bar{\psi}_{\alpha\sigma}\psi_{\alpha\sigma}\right)^2 - \mu\sum_{\alpha=1}^{N}\sum_{\sigma}\bar{\psi}_{\alpha\sigma}\psi_{\alpha\sigma}, \quad (1)$$

$$\mathcal{S}_B = \frac{U}{2}\left(\sum_{\alpha=1}^{N}\sum_{\sigma}\bar{\varphi}_{\alpha\sigma}\varphi_{\alpha\sigma}\right)^2 - \mu\sum_{\alpha=1}^{N}\sum_{\sigma}\bar{\varphi}_{\alpha\sigma}\varphi_{\alpha\sigma}. \quad (2)$$

Here $\psi_{\alpha\sigma}$ and $\bar{\psi}_{\alpha\sigma}$ are fermionic Grassmann variables with the replica index $\alpha = 1, \ldots, N$ and spin σ, and $\varphi_{\alpha\sigma}$ and $\bar{\varphi}_{\alpha\sigma}$ are complex bosonic variables. Note that there is no imaginary-time index in Eqs. (1) and (2). The $(0+0)d$ model with the suppressed imaginary-time index can also be regarded as the effective action of the $(0+1)d$ model. In the Appendix, we show that the $N = 1$ fermionic model is the effective model for a single Matsubara frequency from the $(0+1)d$ Hubbard atom and derive the expressions for the corresponding coupling constants. This suppression simplifies the functional space of the LWF into the function space: the Green's function is a single number, and the bare Green's function G_0 is equal to $G_0 = \mu^{-1}$. These conveniences allow us to easily investigate the analytic structure of its mapping from G_0 to G.

The same model occurs in the replica theory of random matrices, with U being the disorder strength and μ controlling which eigenvalues one is investigating [32]. In that setting physical results are obtained by using the "replica trick," which involves treating N as a continuous noninteger variable and taking the $N \to 0$ limit. In contrast, here we have an exploratory focus and are interested in the LWF's behavior for all N.

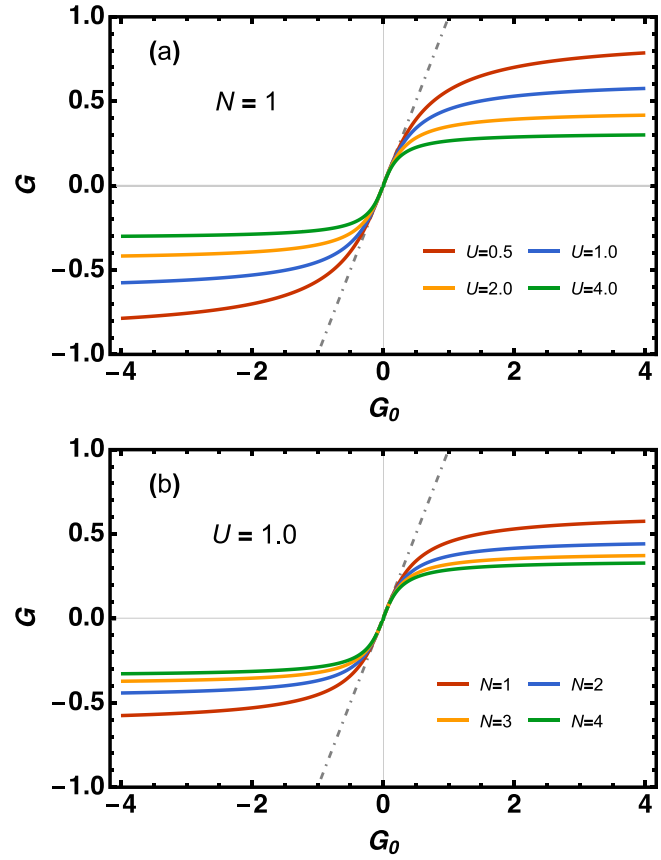

FIG. 1. The interacting Green's function $G[G_0]$ in the bosonic $(0+0)d$ N-replica model. G increases monotonically with G_0, and for each value of G there is a unique value of G_0, showing that the LWF is single valued. In (a), the number of replicas $N = 1$, and the interaction strength $U = 0.5$ (red line; largest absolute values), 1.0 (blue), 2.0 (yellow), and 4.0 (green; smallest absolute values). In (b), the interaction strength $U = 1.0$, and the number of replicas $N = 1$ (red line; largest absolute values), 2 (blue), 3 (yellow), and 4 (green; smallest absolute values). The dot-dashed line shows $G = G_0$.

In spite of the simple function space of the LWF, the N-replica generalization makes the $(0+0)d$ model more realistic toward the $(0+1)d$ Hubbard atom. When we consider the action of the fermionic Hubbard atom in Matsubara frequency space, for example, one can find its formal similarity to the N-replica model:

$$\mathcal{S}_F^{\mathrm{HA}} = \frac{\tilde{U}}{2\beta}\sum_{k}\left(\sum_{n\sigma}\bar{\psi}_{n-k,\sigma}\psi_{n,\sigma}\right)\left(\sum_{m\sigma'}\bar{\psi}_{m+k,\sigma'}\psi_{m,\sigma'}\right) - \sum_{n\sigma}\bar{\psi}_{n\sigma}(i\omega_n + \tilde{\mu})\psi_{n\sigma}, \quad (3)$$

where β and $\tilde{U}$ are the inverse temperature and the strength of Hubbard interaction, respectively, and $\omega_n = (2n+1)\pi/\beta$ is the fermionic Matsubara frequency. When the number of replicas N is taken to be equal to the number of Matsubara frequencies, i.e., countably infinite, with U and μ in Eq. (1) identified with $\tilde{U}/\beta$ and $(i\omega_n + \tilde{\mu})$, the only differences of

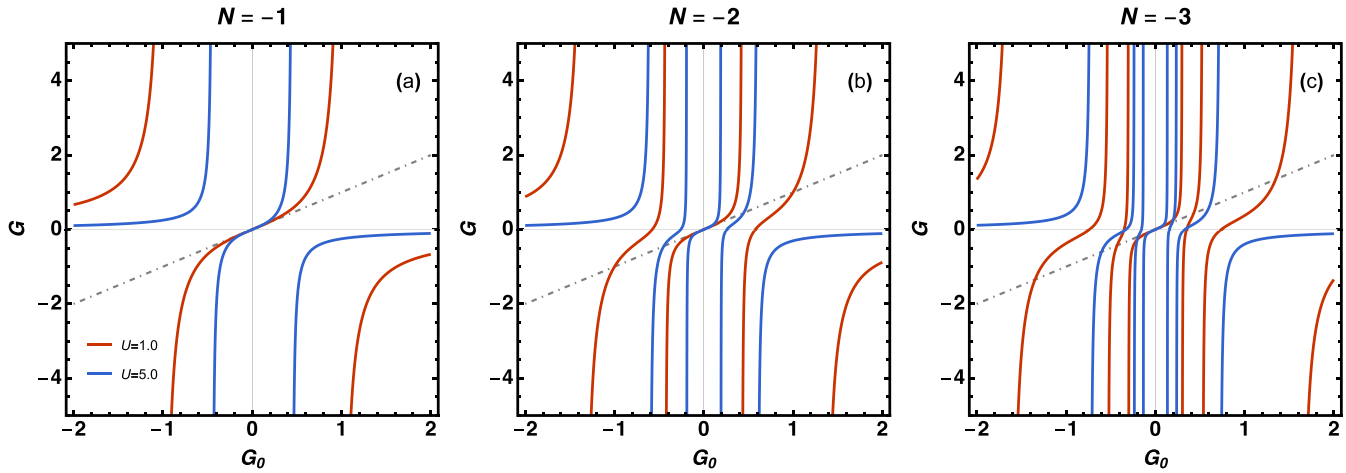

FIG. 2. The interacting Green's function $G[G_0]$ in the fermionic $(0+0)d$ N-replica model. In (a), the model has one replica, G has two poles, and for a given value of $\tilde{G}$ there are two solutions $\tilde{G}_0$ which satisfy $G[\tilde{G}_0] = \tilde{G}$. In (b), there are two replicas and four poles, and for each value of $\tilde{G}$ there are four solutions of $\tilde{G}_0$. In (c), there are three replicas, six poles, and six solutions of $\tilde{G}_0$. Red lines show G with an interaction strength $U = 1.0$, and blue lines show $U = 5.0$. The dot-dashed lines show $G = G_0$.

two models are two simplifications; in the N-replica model the single-particle term's frequency dependence $i\omega_n$ is suppressed, and the zero-energy transfer for the k index ($k = 0$) in the interaction term is selected.

We calculate the fermionic partition function of the $(0+0)d$ model for general N using the combinatorics of the Grassmann variables:

$$\mathcal{Z}_F(N,U,\mu) = \int \prod_{\alpha=1}^{N} \prod_{\sigma=\uparrow,\downarrow} d\bar{\psi}_{\alpha\sigma} d\psi_{\alpha\sigma} \exp\{-\mathcal{S}_F\} = \sum_{n=0}^{N} \frac{1}{n!} \int \prod_{\alpha=1}^{N} \prod_{\sigma=\uparrow,\downarrow} d\bar{\psi}_{\alpha\sigma} d\psi_{\alpha\sigma} (-\mathcal{S}_F)^n$$
$$= \sum_{k=0}^{N} \frac{(2N)!}{(2N-2k)!(k!)} \left(-\frac{U}{2}\right)^k \mu^{2(N-k)} = (2U)^N \mathcal{U}\left(-N, \frac{1}{2}, \frac{\mu^2}{2U}\right). \tag{4}$$

In the second line we used the binomial expansion of $(-\mathcal{S}_F)^n$. The final result is written in terms of $\mathcal{U}$, the Tricomi confluent hypergeometric function, which is defined for both integer and noninteger N. In the case of integer values of the number of replicas N the partition function $\mathcal{Z}_F$ is an Nth-order polynomial in μ^2 and $-U$. It therefore is able to change sign as a function of μ up to $2N$ times, and it never diverges for any finite value of μ^2 and U.

In contrast, the bosonic partition function is always positive. Moreover, it converges only if either $U > 0$ or $U = 0$ and $\mu < 0$:

$$\mathcal{Z}_B(N,U,\mu) = \int \prod_{\alpha=1}^{N} \prod_{\sigma=\uparrow,\downarrow} [d\bar{\varphi}_{\alpha\sigma} d\varphi_{\alpha\sigma}] \exp\{-\mathcal{S}_B\} = \int \prod_{\alpha=1}^{N} \prod_{\sigma=\uparrow,\downarrow} [d\bar{\varphi}_{\alpha\sigma} d\varphi_{\alpha\sigma}] \exp\left\{-\frac{U}{2}\left(\sum_{\alpha\sigma} \bar{\varphi}_{\alpha\sigma}\varphi_{\alpha\sigma}\right)^2 + \mu \sum_{\alpha\sigma} \bar{\varphi}_{\sigma\alpha}\varphi_{\alpha\sigma}\right\}$$
$$= \frac{\Omega_{4N}}{2} \int_0^\infty dQ\, Q^{2N-1} \exp\left\{-\frac{U}{2}Q^2 + \mu Q\right\}$$
$$= \frac{1}{2}\left(\frac{2\pi^2}{U}\right)^N \left[\frac{\Gamma\left(\frac{1}{2}\right)}{\Gamma\left(\frac{1}{2}+N\right)} \mathcal{M}\left(N, \frac{1}{2}, \frac{\mu^2}{2U}\right) + \left(\frac{-\mu}{\sqrt{2U}}\right) \frac{\Gamma\left(-\frac{1}{2}\right)}{\Gamma(N)} \mathcal{M}\left(\frac{1}{2}+N, \frac{3}{2}, \frac{\mu^2}{2U}\right)\right]$$
$$= \frac{1}{2}\left(\frac{2\pi^2}{U}\right)^N \mathcal{U}\left(N, \frac{1}{2}, \frac{\mu^2}{2U}\right). \tag{5}$$

Here $\mathcal{M}$ and Γ denote the Kummer confluent hypergeometric function and the gamma function, respectively. In the second line of Eq. (5), $Q = \sum_{\alpha\sigma} \bar{\varphi}_{\alpha\sigma}\varphi_{\alpha\sigma}$, and Ω_{4N} is the solid angle of the $4N$-dimensional sphere, which can be expressed in terms of the gamma function as $2\pi^{2N}/\Gamma(2N)$. A comparison of the final result for the bosonic $\mathcal{Z}_B(N,U,\mu)$ with the fermionic $\mathcal{Z}_F(N,U,\mu) = (2U)^N \mathcal{U}(-N, \frac{1}{2}, \frac{\mu^2}{2U})$ shows that, up to a normalization constant that is independent of μ, the bosonic and fermionic results are the same Tricomi confluent hypergeometric function $\mathcal{U}$, with the only difference being $N \to -N$.

It is worth noting that the $N \to -N$ correspondence between bosonic and fermionic results is well known in the literature of replicas. This correspondence is natural because a Gaussian integral with commuting variables produces an inverse determinant, while a Gaussian integral with Grassmann

variables produces a determinant. It is also common to treat the number of replicas N as a real variable; this is the foundation of the replica trick where N is analytically continued to $N = 0$.

Next, we calculate the Green's function:

$$G_F = \frac{1}{2N}\frac{\partial}{\partial\mu}\ln\mathcal{Z}_F = \frac{\mu}{2U}\frac{\mathcal{U}(1-N,3/2,\mu^2/2U)}{\mathcal{U}(-N,1/2,\mu^2/2U)}, \tag{6}$$

$$G_B = -\frac{1}{2N}\frac{\partial}{\partial\mu}\ln\mathcal{Z}_B = \frac{\mu}{2U}\frac{\mathcal{U}(1+N,3/2,\mu^2/2U)}{\mathcal{U}(N,1/2,\mu^2/2U)}. \tag{7}$$

Here we find an exact correspondence between bosonic and fermionic results under the transformation $N \to -N$. There is, however, an immense difference between the bosonic $+N$ case and the fermionic $-N$ case: since the bosonic partition function $\mathcal{Z}_B$ is positive definite and is finite (if $U > 0$), the bosonic Green's function has no isolated pole. In contrast, the sign of the fermionic partition function $\mathcal{Z}_F$ can change as many as $2N$ times, each of which causes a pole in the fermionic Green's function.

In order to analyze the number of branches of the LWF, we express the interacting Green's function G as a function of the noninteracting Green's function $G_0 = \mu^{-1}$:

$$G[N,U;G_0] = \frac{1}{2G_0U}\frac{\mathcal{U}\left(1+N,3/2,1/2G_0^2U\right)}{\mathcal{U}\left(N,1/2,1/2G_0^2U\right)}. \tag{8}$$

The LWF is free from the multivaluedness problem if for every value of G there is only one value of G_0 which produces that value.

III. RESULTS

In Fig. 1 we plot the bosonic $G[N,U;G_0]$ for various U and N values. The map $G_0 \mapsto G$ is always injective for all positive N and U values investigated. Using Eqs. (5) and (7), one can analytically show that $G[G_0]$ increases monotonically with G_0 for the finite-U bosonic case:

$$\frac{dG_B[N,U;G_0]}{dG_0} = \frac{1}{2NG_0^2}\left[\frac{1}{\mathcal{Z}_B}\frac{\partial^2\mathcal{Z}_B}{\partial\mu^2} - \frac{1}{\mathcal{Z}_B^2}\left(\frac{\partial\mathcal{Z}_B}{\partial\mu}\right)^2\right]$$
$$= \frac{1}{2NG_0^2}\left[\langle Q^2\rangle_{\mathcal{S}_B} - \langle Q\rangle_{\mathcal{S}_B}^2\right] \geqslant 0, \tag{9}$$

where $\langle\cdots\rangle_{\mathcal{S}_B}$ is the statistical average over the bosonic action $\mathcal{S}_B$.

The injective map implies the well-defined Legendre transformation of the thermodynamic potential. In fact, the thermodynamic potential is a convex function with respect to μ of a fixed sign. So the Legendre transformation for a given sign of μ is well defined. Furthermore, since μ-positive and -negative (or, equivalently, positive and negative G_0) branches map to G of different signs, the injective mapping from $G_0 \mapsto G$ is preserved for all signs of G_0. Recently, the mathematical proof of the well-defined LWF in the classical Euclidean lattice field theory appeared [21,33], which is relevant to the bosonic system in our study.

The well-defined LWF in the bosonic case is in contrast to the fermionic one where the map is not injective. Figure 2 shows the fermionic $G_0 \mapsto G$ mapping for three different integer N values: $N = -1$, -2, and -3. For $N = -1$, there exist one positive and one negative $\tilde{G}_0$ for a given $\tilde{G}$, which satisfy $G[\tilde{G}_0] = \tilde{G}$. The number of both positive and negative solutions increases by 1 as we decrease N by 1. So the total increase in the number of solutions is 2 for an additional replica index. As we decrease N by 1, the number of poles along the real axis increases by 2, which is the same increase as the number of solutions. And poles along the real axis correspond to the sign change of the partition function.

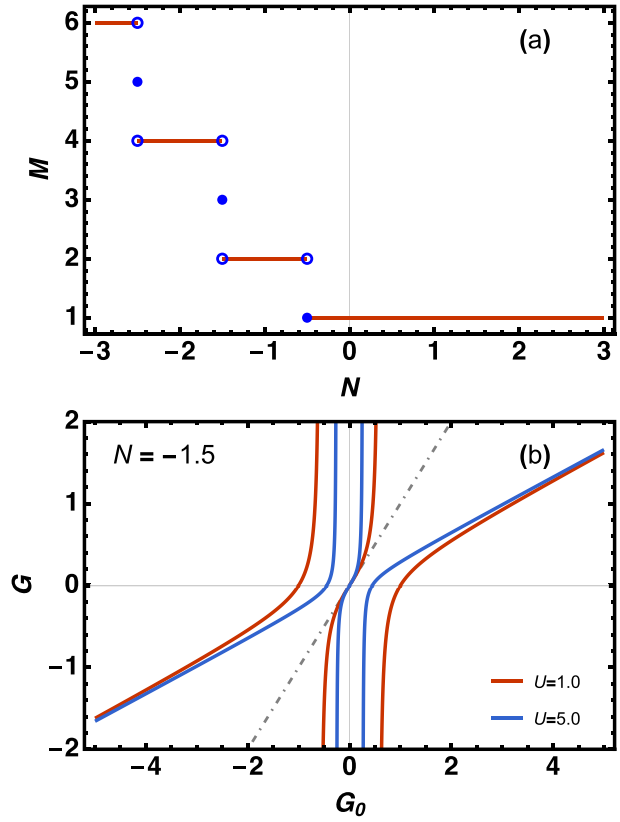

FIG. 3. (a) M, the number of G_0 values that give the same value of G, as a function of the number of replicas N, in the $(0+0)d$ N-replica model. Negative values of N on this graph represent results from the fermionic model with $|N|$ replicas, while positive values represent the behavior of the bosonic model. N is treated as a continuous variable because the fermionic and bosonic partition functions are a hypergeometric function that is defined for a general real N. At negative half-integers the number of solutions M value is odd and is represented as solid blue dots. (b) shows the case of $N = -3/2$, where there are three values of G_0 that give the same value of G. G diverges proportionally to G_0 at large $|G_0| \gg 1$. Red lines show G with an interaction strength $U = 1.0$, and blue lines show $U = 5.0$. The dot-dashed line shows $G = G_0$.

The evolution of the number of solutions M as a function of N is shown in Fig. 3(a). In Fig. 3(a), the number of replica indices is generalized to the real number instead of the integer. A clear steplike increase in M is observed only on the fermionic side with the negative N. On the N axis, the discontinuous change in M occurs at the negative half-integers: $-1/2$, $-3/2$, $-5/2$, and so on. The $N = -1/2$ case corresponds to the spinless system with a vanishing interacting term since the total number of indices becomes unity and the self-interaction term vanishes due to the fermionic

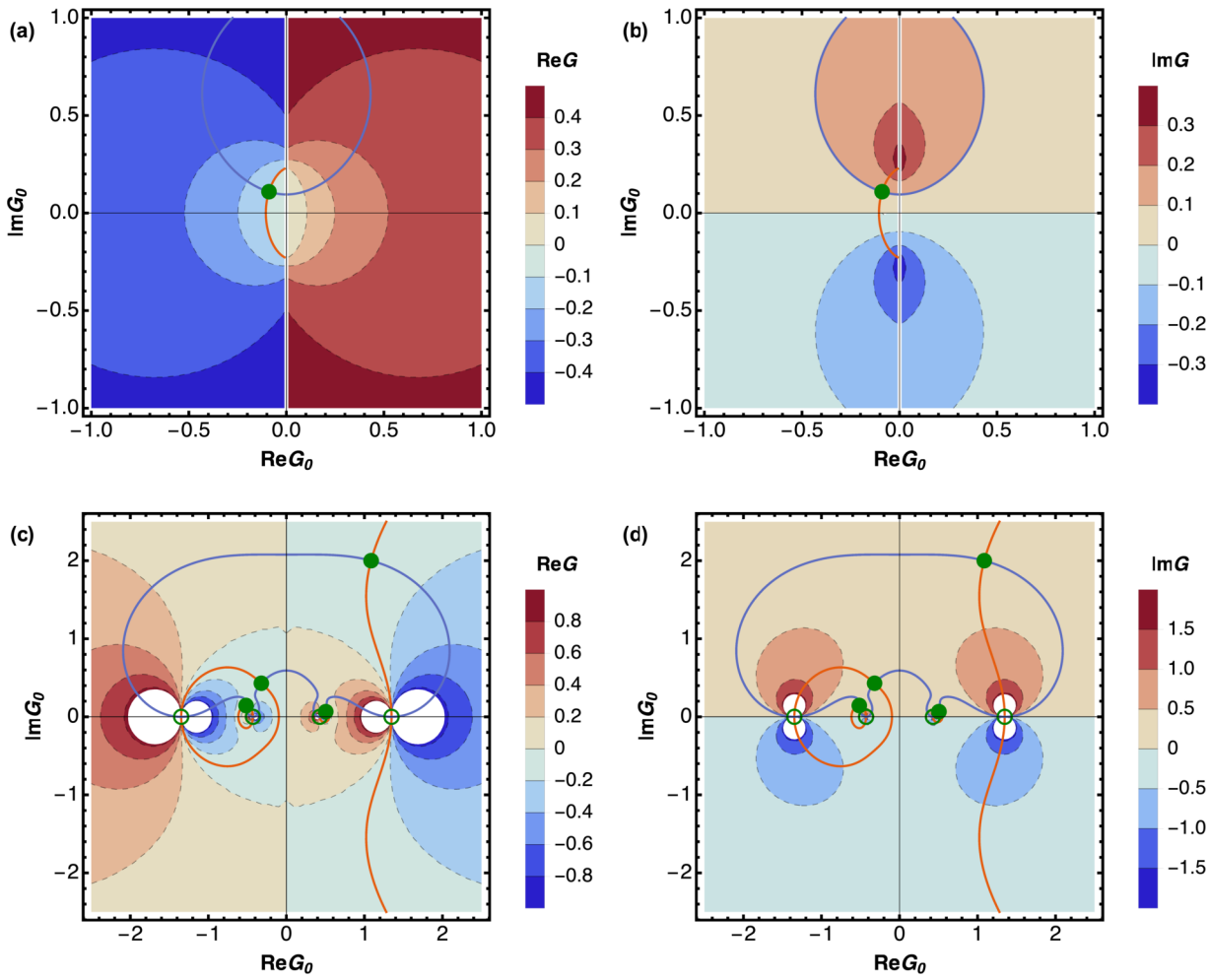

FIG. 4. $G[G_0]$ when both G and G_0 are complex, with solid green dots placed at the solutions of $G[\tilde{G}_0] = \tilde{G}$. Contours of Re$G$ are shown on the left and contours of ImG are shown on the right. The bosonic G is shown in the top panels, with a red line at Re$G = -0.1$, a blue line at Im$G = 0.1$, and a solid green dot at the $\tilde{G}_0$ solution for $G[\tilde{G}_0] = \tilde{G} = -0.1 + 0.1i$. The fermionic G is shown in the bottom panels, with red lines at Re$G = -0.1$, blue lines at Im$G = 0.35$, and four solid green dots at the four $\tilde{G}_0$ solutions for $G[\tilde{G}_0] = \tilde{G} = -0.1 + 0.35i$. The open green dots are located at singularities of G and do not solve $G[\tilde{G}_0] = \tilde{G}$. The number of replicas $|N| = 2$ in all panels, and the interaction strength $U = 1.0$.

statistics. So the interacting Green's function G becomes the same as the noninteracting Green's function G_0. For a negative half-integer N smaller than $-1/2$, the outermost G branch, whose range spans $(-\infty, \infty)$ instead of $(0, \infty)/(-\infty, 0)$, appears, giving additional $\tilde{G}_0$ for a given $\tilde{G}$. Figure 3(b) presents the $N = -3/2$ case, where $M = 3$ for $U = 1$ and 5.

Motivated by G_0 and G being complex functions in Matsubara frequency space in the $(0+1)d$ Hubbard atom [Eq. (3)], we now generalize the domain of the mapping $G_0 \mapsto G$ to a complex number for the N-replica model. Figure 4 shows the contour plot of the real and imaginary parts of G on the complex G_0 plane for both the bosonic ($N = 2$) and fermionic ($N = -2$) cases. For a given $\tilde{G}$ the Re$\tilde{G}$ contour is highlighted by a red line, and the Im$\tilde{G}$ contour is highlighted by a blue line. The solution $\tilde{G}_0$ which satisfies $G[\tilde{G}_0] = \tilde{G}$ appears as an intersection of two contour lines for real and imaginary parts of $\tilde{G}$.

As we gradually introduce the imaginary part to $\tilde{G}$, the $\tilde{G}_0$ solutions evolve to a general complex number from the real number. In general, the number of solutions is preserved in the presence of the imaginary part of $\tilde{G}$. One can find a single intersection for the bosonic case ($N = 2$), marked as a green solid circle, but four different solutions for the fermionic case ($N = -2$). Note that four additional intersections are marked with open circles for the fermionic case, but they are not true solutions because they lie at singularities where ReG changes discontinuously from $+\infty$ to $-\infty$.

When $\tilde{G}$ becomes purely imaginary, which corresponds to the half-filled fermionic Hubbard atom with the purely imaginary interacting Green's function of Eq. (3),

$$G_F^{\mathrm{HA}}(i\omega_n) = -\frac{i\omega_n}{\omega_n^2 + \tilde{U}^2/4}, \tag{10}$$

two different $\tilde{G}_0$ solutions can be degenerate. In the Appendix one can find the explicit relation between the coupling constants of the half-filled Hubbard atom and the $N = 1$ fermionic replica model. Supposing a purely imaginary μ_{phys} and $\tilde{G}_{0,\mathrm{phys}} = 1/\mu_{\mathrm{phys}}$, the physical interacting Green's function $\tilde{G}_{\mathrm{phys}}$ is also purely imaginary. However, there exists an additional unphysical solution $\tilde{G}_{0,\mathrm{unphys}}$ which is purely

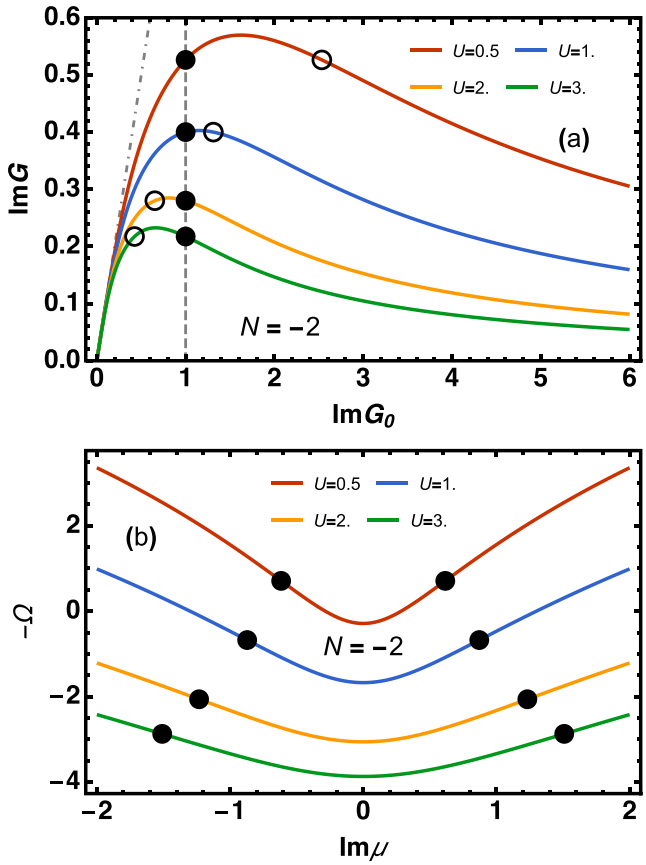

FIG. 5. (a) Fermionic interacting Green's function as a function of the purely imaginary noninteracting Green's function for $N = -2$. Red, blue, orange, and green lines represent $U = 0.5$, 1.0, 2.0, and 3.0, respectively. Black solid dots show the physical solutions $(\tilde{G}_{0,\mathrm{phys}}, \tilde{G}_{\mathrm{phys}})$ for a given imaginary chemical potential $\mu = -i$ with various U values. Black open symbols present the purely imaginary unphysical solutions $(\tilde{G}_{0,\mathrm{unphys}}, \tilde{G}_{\mathrm{phys}})$. As we increase U, $\tilde{G}_{0,\mathrm{unphys}}$ crosses $\tilde{G}_{0,\mathrm{phys}}$ at $U_c \sim 1.317$. The dash-dotted line shows $G = G_0$. (b) The fermionic thermodynamic potential (with minus sign) as a function of the purely imaginary chemical potential for various U values. Black solid dots present the inflection points of the thermodynamic potential. Two inflection points for a given U separate the domain of $G_0 \mapsto G$ (or $\mu \mapsto G$) mapping into three.

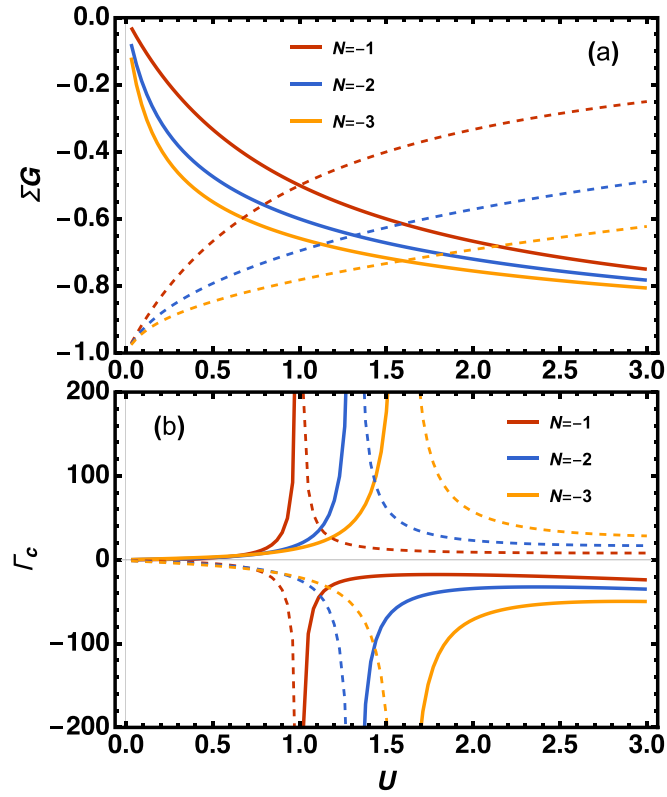

FIG. 6. (a) Evolution of the fermionic $\Sigma[\tilde{G}_{\mathrm{phys}}]\tilde{G}_{\mathrm{phys}}$ for two different $\tilde{G}_0$ branches. Solid (dashed) lines present for the physical (unphysical) branches. The physical branches are connected to the noninteracting limit, $\Sigma G = 0$. There exists a branching point between the physical and unphysical branches for each N value. and it becomes larger as we increase $|N|$ values. (b) The fermionic charge vertex as a function of U for various numbers of replicas N. The charge vertex for both physical and unphysical branches diverges at the branching point of the self-energy. The physical noninteracting Green's function $\tilde{G}_{0,\mathrm{phys}}$ is fixed as i.

imaginary. Figure 5(a) shows the evolution of $\tilde{G}_{0,\mathrm{unphys}}$ as a function of U for the $N = -2$ case. As we increase the U values, $\tilde{G}_{0,\mathrm{unphys}}$ approaches $\tilde{G}_{0,\mathrm{phys}}$ from higher absolute values and eventually becomes degenerate at U_c. For $U > U_c$, the absolute value of $\tilde{G}_{0,\mathrm{unphys}}$ becomes smaller than $\tilde{G}_{0,\mathrm{phys}}$. One can find the crossing of $\tilde{G}_{0,\mathrm{phys}}$ and $\tilde{G}_{0,\mathrm{unphys}}$ at $U_c \sim 1.317$.

The origin of the multiple branches along the imaginary axis is the lack of the convexity of the thermodynamic potential as a function of the chemical potential μ. Figure 5(b) shows two inflection points in the thermodynamic potential, $\Omega = -\ln\mathcal{Z}$. Since the Legendre transform is the value-to-slope mapping, two inflection points separate the domain of the $G_0(\mu) \mapsto G$ mapping into three pieces, and for a given sign of $\tilde{G}$ (or for a given sign of slope of Ω as a function of $\mathrm{Im}\mu$), two of three G_0 domains incorporate $\tilde{G}$ in the corresponding image. The existence of the physical and unphysical solutions $\tilde{G}_0$ is the manifestation of such a domain structure.

We now show how the physical and unphysical $\tilde{G}_0$ solutions manifest themselves in the self-energy and the charge vertex as a function of U. Figure 6(a) presents $\Sigma[\tilde{G}_{\mathrm{phys}}]\tilde{G}_{\mathrm{phys}}$ for two different solutions. The self-energy is defined as a function of G, $\Sigma[G] = 1/G_0[G] - 1/G$. While the physical self-energy is connected to the physical noninteracting limit, $\Sigma = 0$, the unphysical self-energy has a finite value even when $U = 0$. As we increase interaction strength U, two self-energy solutions cross each other at the branching point U_c. Beyond the branching point, the unphysical solution generates the less correlated self-energy with smaller absolute values, and this is the reason why the bold-series representation selects the unphysical branches beyond the branching points. The branching point U_c increases as a function of the number of replicas $|N|$.

At this branching point, the charge vertex defined as

$$\Gamma_c[G] = \frac{d\Sigma[G]}{dG} = -\frac{1}{G_0[G]^2}\frac{dG_0[G]}{dG} + \frac{1}{G^2} \tag{11}$$

shows the divergence with a polelike sign change. Compared to the physical vertex, the unphysical one has the opposite sign. This divergence originates from the $dG_0[G]/dG$ factor.

In Fig. 5(a), one can find the diverging dG_0/dG when $G_{0,\mathrm{phys}}$ and $G_{0,\mathrm{unphys}}$ become degenerate. This behavior captures well the divergent vertex in a $(0+1)d$ Hubbard atom [28,29]. Note that in the N-replica model the vertex is a simple number without the matrix structure. So the classification of divergence using the eigenvector locality of the vertex matrix [28] cannot be applied to the N-replica model.

We also emphasize that there exist additional unphysical $\tilde{G}_{0,\mathrm{unphys}}$ away from the imaginary axis for $N \leqslant -2$ for a purely imaginary $\tilde{G}_{\mathrm{phys}}$. Those additional solutions, however, do not become degenerate with $\tilde{G}_{0,\mathrm{phys}}$, so there is no corresponding divergence of the charge vertex in the N-replica model. The number of those nonsingular solutions scales in the form of $2|N|-2$ and becomes infinite in the $|N| \to \infty$ limit. Those $2|N|-2$ complex unphysical solutions reproduce the existence of the unphysical branches with a finite real part, reported in the $(0+1)d$ Hubbard atom [28]. Along the same lines, we can exclude the possible divergence of the charge vertex in the $(0+0)d$ bosonic system since there exists only one physical $\tilde{G}_{0,\mathrm{phys}}$ solution for a given $\tilde{G}_{\mathrm{phys}}$.

IV. CONCLUSION

We exactly solved the $(0+0)d$ model with a general number of replicas for both bosons and fermions. It turns out that both the bosonic and fermionic Green's functions can be written in terms of the Tricomi confluent hypergeometric function, but with different signs of the number of replicas index N. We show that the multivaluedness of the LWF is observed only for the fermionic model not the bosonic one, implying a direct link to the fermionic statistics. Especially, the sign oscillation and the lack of the log convexity of the partition function are the characteristic features of the fermionic statistics in the $(0+0)d$ N-replica model. In the fermionic model, the multiple G_0 result in the same G, and the number of G_0 increases proportional to the number of replicas. For a complex G, the multiple G_0 evolve into complex numbers. We found the interesting case where two purely imaginary G_0 can be degenerate, at which the charge vertex diverges in a polelike manner.

Despite its simple form, the $(0+0)d$ N-replica model's qualitative behavior shows several remarkable similarities to that of the $(0+1)d$ Hubbard atom. First of all, the convergence of the bold series to the unphysical branch in the N-replica model can be understood in terms of the crossing of the physical and unphysical G_0 of the $(0+0)d$ model. For purely imaginary $\tilde{G}$, two out of $2|N|$ solutions are aligned on the imaginary axis and cross each other at $U = U_c$. Since the bold series always chooses the weakly interacting Σ, the bold series converges to the unphysical branch for $U > U_c$. The infinite number of solutions of the LWF observed in Ref. [28] naturally appears in the N-replica model in the $|N| \to \infty$ limit. In the N-replica model, the total number of branches scales as $2|N|$ as $|N| \to \infty$. And there exist an infinite number of complex G_0 which have a nontrivial real part for a purely imaginary G. The half-filled Hubbard atom shows that there appear G_0 showing the nontrivial real part in contrast to the physical G_0, which is purely imaginary [28].

Furthermore, our model suggests that the bold series for the bosonic case is promising. Throughout our study, the bosonic model showed the well-defined LWF without the multivaluedness problem. Our results give a positive signal to the bosonic bold diagrammatic Monte Carlo method, whose major concern is the possible multivaluedness problem.

ACKNOWLEDGMENTS

A.J.K. was supported by EPSRC Grant No. EP/P003052/1, and V.S. was supported by EPSRC Grant No. EP/M011038/1. We thank L. Du, A. Toschi, V. Olevano, C. Weber, E. Plekhanov, R. Rossi, F. Werner, H. Kim, L. Reining, P. Werner, E. Kozik, and B. Svistunov for fruitful discussions. V.S. thanks King's College London for hospitality.

APPENDIX: EFFECTIVE ACTION OF THE FERMIONIC HUBBARD ATOM FOR A SINGLE MATSUBARA FREQUENCY

In this Appendix, we derive the effective action for a given Matsubara frequency from the $(0+1)d$ Hubbard atom and show that it corresponds to the $N=1$ fermionic replica model. By integrating out the Grassmann variables of the partition function of the Hubbard atom except those of a certain Matsubara frequency, $\bar{\psi}_{n\sigma}$ and $\psi_{n\sigma}$,

$$\begin{aligned}\mathcal{Z}_F^{\mathrm{HA}} &= \int \prod_{n,\sigma} \mathcal{D}[\bar{\psi}_{n\sigma}, \psi_{n\sigma}] \exp\left[-\mathcal{S}_F^{\mathrm{HA}}\right] \\ &= \mathcal{Z}'_n \int \prod_{\sigma} \mathcal{D}[\bar{\psi}_{n\sigma}, \psi_{n\sigma}] \exp\left[-\mathcal{S}_{\mathrm{eff}}^{(n)}\right], \end{aligned} \tag{A1}$$

one can formally express the effective action $\mathcal{S}_{\mathrm{eff}}^{(n)}$ for the selected Matsubara frequency. Due to the Grassmann algebra, $\mathcal{S}_{\mathrm{eff}}^{(n)}$ is composed of terms only up to quartic interaction as

$$\mathcal{S}_{\mathrm{eff}}^{(n)} = \frac{\Gamma_n}{2}\left(\sum_\sigma \bar{\psi}_{n\sigma}\psi_{n\sigma}\right)^2 - G_{0,n}^{-1}\sum_\sigma \bar{\psi}_{n\sigma}\psi_{n\sigma}. \tag{A2}$$

Note that $\bar{\psi}_{n\sigma}\psi_{n\bar{\sigma}}$ terms are not allowed since the spin is a conserved quantity. At this level, it is already clear that the $N=1$ fermionic replica model can be viewed as an effective action of the $(0+1)d$ Hubbard atom by identifying $G_{0,n}^{-1}$ and Γ_n with μ and U in Eq. (1).

To be more accurate, we explicitly calculate $G_{0,n}^{-1}$ and Γ_n for the half-filled case. At half-filling where $\tilde{\mu} = \tilde{U}/2$ in Eq. (3), one can fix Γ_n and $G_{0,n}^{-1}$ using the known analytic expressions of the Green's function,

$$G^{\mathrm{HA}}(i\omega_n) = -\frac{i\omega_n}{\omega_n^2 + \tilde{U}^2/4}, \tag{A3}$$

and the particle-hole susceptibility of the magnetic channel [34],

$$\begin{aligned}\frac{1}{\beta}\chi_{\mathrm{ph,m}}^{\mathrm{HA}} &= \frac{1}{\omega_n^2+\tilde{U}^2/4} + \left[\frac{1}{\beta\tilde{U}} + \frac{1}{2}\tanh\left(\frac{\beta\tilde{U}}{4}\right)\right] \\ &\quad\times \frac{\tilde{U}^2}{\left[\omega_n^2+\tilde{U}^2/4\right]^2} - \frac{\tilde{U}^3/\beta}{\left[\omega_n^2+\tilde{U}^2/4\right]^3}. \end{aligned} \tag{A4}$$

The resulting parameters of the effective action are written as

$$G_{0,n}^{-1} = \frac{i\omega_n}{X\left(n, \frac{\beta\tilde{U}}{2}\right)}, \quad \Gamma_n = \frac{\omega_n^2 + \tilde{U}^2/4}{X\left(n, \frac{\beta\tilde{U}}{2}\right)} - \frac{\omega_n^2}{X^2\left(n, \frac{\beta\tilde{U}}{2}\right)}, \tag{A5}$$

where $X(n, \beta\tilde{U}/2)$ is a dimensionless real function whose expression is

$$X\left(n, \frac{\beta\tilde{U}}{2}\right) = 1 + \frac{\tilde{U}/\beta}{\omega_n^2 + \tilde{U}^2/4} + \frac{\tilde{U}^2}{2\left[\omega_n^2 + \tilde{U}^2/4\right]} \tanh\left(\frac{\beta\tilde{U}}{4}\right) - \frac{\tilde{U}^3/\beta}{\left[\omega_n^2 + \tilde{U}^2/4\right]^2}. \tag{A6}$$

Equations (A5) and (A6) show that at half-filling the corresponding μ and U in the $N = 1$ fermionic model are purely imaginary and positive real, respectively, where we observe the branching point of the LWF.

[1] J. M. Luttinger and J. C. Ward, Phys. Rev. **118**, 1417 (1960).
[2] J. M. Luttinger, Phys. Rev. **119**, 1153 (1960).
[3] A. Georges, G. Kotliar, W. Krauth, and M. J. Rozenberg, Rev. Mod. Phys. **68**, 13 (1996).
[4] T. A. Maier, M. Jarrell, T. Prushke, and M. Hettler, Rev. Mod. Phys. **77**, 1027 (2005).
[5] A. N. Rubtsov, M. I. Katsnelson, and A. I. Lichtenstein, Phys. Rev. B **77**, 033101 (2008).
[6] G. Rohringer, A. Toschi, A. Katanin, and K. Held, Phys. Rev. Lett. **107**, 256402 (2011).
[7] L. Pollet, N. V. Prokof'ev, and B. V. Svistunov, Phys. Rev. B **83**, 161103(R) (2011).
[8] P. Staar, T. A. Maier, and T. C. Schulthess, Phys. Rev. B **88**, 115101 (2013).
[9] J. Gukelberger, E. Kozik, and H. Hafermann, Phys. Rev. B **96**, 035152 (2017).
[10] G. Kotliar, S. Y. Savrasov, K. Haule, V. S. Oudovenko, O. Parcollet, and C. A. Marianetti, Rev. Mod. Phys. **78**, 865 (2006).
[11] V. I. Anisimov, A. I. Poteryaev, M. A. Korotin, A. O. Anokhin, and G. Kotliar, J. Phys.: Condens. Matter **9**, 7359 (1997).
[12] N. Prokof'ev and B. Svistunov, Phys. Rev. Lett. **99**, 250201 (2007).
[13] N. V. Prokof'ev and B. V. Svistunov, Phys. Rev. B **77**, 125101 (2008).
[14] K. Van Houcke, E. Kozik, N. Prokof'ev, and B. Svistunov, Phys. Proc. **6**, 95 (2010).
[15] E. Kozik, K. Van Houcke, E. Gull, L. Pollet, N. Prokof'ev, B. Svistunov, and M. Troyer, Europhys. Lett. **90**, 10004 (2010).
[16] S. Biermann, F. Aryasetiawan, and A. Georges, Phys. Rev. Lett. **90**, 086402 (2003).
[17] C. De Dominicis and P. C. Martin, J. Math. Phys. **5**, 14 (1964).
[18] R. Chitra and G. Kotliar, Phys. Rev. B **63**, 115110 (2001).
[19] M. Potthoff, Eur. Phys. J. B **32**, 429 (2003).
[20] M. Potthoff, Condens. Matter Phys. **9**, 557 (2006).
[21] L. Lin and M. Lindsey, arXiv:1809.02901.
[22] G. Baym and L. P. Kadanoff, Phys. Rev. **124**, 287 (1961).
[23] G. Baym, Phys. Rev. **127**, 1391 (1962).
[24] E. Kozik, M. Ferrero, and A. Georges, Phys. Rev. Lett. **114**, 156402 (2015).
[25] R. Rossi and F. Werner, J. Phys. A **48**, 485202 (2015).
[26] A. Stan, P. Romaniello, S. Rigamonti, L. Reining, and J. A. Berger, New J. Phys. **17**, 093045 (2015).
[27] W. Tarantino, P. Romaniello, J. A. Berger, and L. Reining, Phys. Rev. B **96**, 045124 (2017).
[28] O. Gunnarsson, G. Rohringer, T. Schäfer, G. Sangiovanni, and A. Toschi, Phys. Rev. Lett. **119**, 056402 (2017).
[29] T. Schäfer, G. Rohringer, O. Gunnarsson, S. Ciuchi, G. Sangiovanni, and A. Toschi, Phys. Rev. Lett. **110**, 246405 (2013).
[30] K. B. Dave, P. W. Phillips, and C. L. Kane, Phys. Rev. Lett. **110**, 090403 (2013).
[31] P. Chalupa, P. Gunacker, T. Schäfer, K. Held, and A. Toschi, Phys. Rev. B **97**, 245136 (2018).
[32] A. Kamenev and M. Mézard, J. Phys. A **32**, 4373 (1999).
[33] L. Lin and M. Lindsey, arXiv:1809.02900.
[34] P. Thunström, O. Gunnarsson, S. Ciuchi, and G. Rohringer, Phys. Rev. B **98**, 235107 (2018).